Optical black hole lasers

Daniele Faccio[1]**, Tal Arane**[1]**, Marco Lamperti**[1] **and Ulf Leonhardt**[2]

[1] School of Engineering and Physical Sciences, SUPA, Heriot-Watt University, EH14 7JG, Edinburgh, UK
[2] School of Physics and Astronomy, University of St Andrews, North Haugh, St Andrews KY16 9SS, UK

E-mail: d.faccio@hw.ac.uk

Abstract

Using numerical simulations we show how to realize an optical black hole laser, i.e. an amplifier formed by travelling refractive index perturbations arranged so as to trap light between a white and a black hole horizons. The simulations highlight the main features of these lasers: the growth inside the cavity of positive and negative frequency modes accompanied by a weaker emission of modes that occurs in periodic bursts corresponding to the cavity round trips of the trapped modes. We then highlight a new regime in which the trapped mode spectra broaden until the zero-frequency points on the dispersion curve are reached. Amplification at the horizon is highest for zero-frequencies, therefore leading to a strong modification of the structure of the trapped light. For sufficiently long propagation times, lasing ensues only at the zero-frequency modes.

PACS numbers: 04.70.−s, 04.70.Dy, 42.65.Re, 42.65.Hw, 41.20.−q

S Online supplementary data available from stacks.iop.org/CQG/29/224009/mmedia

(Some figures may appear in colour only in the online journal)

1. Introduction

Since Unruh's first suggestion that flowing media can be used as analogues for gravity [1] and in particular for studying certain physical phenomena usually associated with gravitational event horizons, e.g. Hawking radiation, the field has seen a steady increase in the number of proposed physical systems in which to observe such effects [2, 3]. Originally, analogue gravity was proposed in systems that physically display a flowing medium that reproduces the flow of space close to a black hole: a flowing fluid that exhibits a gradient from subsonic to supersonic flow presents a point within the gradient such that the flow speed equals the speed of acoustic waves. This is a point of non-return for acoustic waves trying to propagate against the flow and is the analogue of an event horizon, causally disconnecting two separate regions

within the medium. Such horizons are much more than mere toys or superficial analogies: they can truly reproduce the kinematics of gravitational event horizons. This implies that a direct analogue of the amplification of vacuum fluctuations and consequent emission of particles away from the horizon, known as Hawking radiation, should be visible. This idea has of course attracted significant attention along with the proposal of various systems that may enhance the Hawking emission [3]. The main point is that the Hawking emission is predicted to occur with a blackbody distribution with a temperature T connected to the horizon through the so-called surface gravity, κ, i.e. the gradient of the gravitational field across the horizon [4, 5]. In analogue systems, the surface gravity is determined by the gradient of the medium flow across the horizon and the combination of steep gradients along with very cold environments (in order to reduce the background thermal noise) is expected to lead to the observation of the spontaneous Hawking emission. Recently, Philbin *et al* proposed an optical analogue for horizons in which the steep gradients are ensured by shock front formation in intense optical pulses and the reduction of the background thermal noise is ensured by the fact that at optical frequencies, room temperature thermal noise is completely negligible [6].

In analogue models, black holes and their time-reversed realization, i.e. white holes [7] play equivalently important roles. Whilst gravitational white holes are expected to be extremely rare, or even non-existent, analogue models abound with ways to generate such objects. Most notably, recent experiments performed in the presence of a white hole horizon in flowing water highlighted a stimulated frequency conversion process that can be considered as the classical limit of Hawking emission [8, 9] whilst an optically induced white hole horizon was used to observe both the classical shifting of light frequency [6, 10–12] and the spontaneous emission of photons [13, 14] that has stimulated an ongoing discussion regarding the precise origin of the emission [15–17].

A remarkable prediction that emerged from analogue gravity studies was the prediction that a combination of a black hole and a white hole event horizons would lead to a feedback amplification process very similar to a laser where radiation is continuously bounced back and forth between the two horizons and hence exponentially amplified [18].

Black hole lasers were first proposed for systems that exhibit a 'superluminal' dispersion relation (i.e. in which the group velocity increases with frequency) such as, for example, Bose–Einstein condensates (BECs). Black hole lasing has subsequently been studied both theoretically and numerically in BEC systems and similar settings [18–21]. In this work we present a numerical study of black hole lasing in optical systems. Our numerics account for realistic parameters of the medium and highlight a laser amplification mechanism that is similar to that studied in BECs. However, we also show that as evolution ensues, the laser develops low-frequency components that eventually seed amplification at what we call the 'zero-frequency' modes. This amplification regime is exponentially favoured over the traditional black hole laser regime and leads to a significant increase in the output radiation. We then highlight and study how the low-frequency (close to zero) region of the spectrum determines the properties of the high-frequency emission, a feature that is expected to be generic to all analogue horizon systems.

2. Optical horizon analogues

Optically induced horizon analogues are based on the use of nonlinear optics to create an effective moving medium [6, 14, 22]. An intense laser pulse with a carrier frequency ω_p, typically in the near-infrared or visible region, is focused into a dielectric medium and through the nonlinear Kerr effect it will excite a material polarisation response that contains two terms. One term oscillates at frequency $2\omega_p$ and may excite photons from the vacuum state under the

condition that energy and momentum conservation relations are satisfied. Unless a particular care is taken in order to enforce such conditions, this so-called four-wave-mixing term (four elementary excitations are involved, two from the input pulse and two from the vacuum state) will be very strongly suppressed [23]. There is a second term that follows the envelope of the input pulse, i.e. it responds to the dc component of the electromagnetic field and is described in terms of the variation of the medium refractive index, $n = n_0 + n_2 I(\zeta)$, where n_0 is the background refractive index ($n_0 \sim 1.45$ in most glasses) and n_2 is the nonlinear refractive, also called the 'Kerr' index of the medium and $\zeta = z - vt$ is the local longitudinal coordinate. $I(\zeta)$ is the propagating intensity (envelope) profile of the laser pulse. In most common media $n_2 \sim 10^{-16}$ W cm^{-2} so that the maximum index variation, $\delta n_{\max} \sim 0.005 - 0.0001$, depending on the laser pulse intensity. With other media it may be possible to obtain higher δn, e.g. some so-called soft glasses or media such as graphene are expected to give values larger by an order of magnitude or more.

Light travels slower in high refractive index regions and faster in low refractive regions, so the moving laser pulse creates a moving δn that locally slows light down. The effective spacetime metric associated with the moving δn is the so-called Gordon metric [24, 25] and may be recast in a form that tightly resembles the Painlevé–Gullstrand metric for black holes [26, 27, 13]. In other words, in the reference frame comoving with the δn, space is flowing with velocity $V = \gamma^2 v(n^2 - 1)/n$: on the leading edge of the perturbation space flows inwards with increasing velocity until $V = c$ (i.e. $v = c/n$) and a black hole horizon is formed. On the trailing edge, the time-reversed situation is verified with space flowing outwards at a decreasing velocity and when $V = c$ a white hole horizon is formed (see also [22]).

In the presence of dispersion, i.e. of a frequency dependence of the medium background refractive index, one must take care in defining the exact nature of the horizon due to the fact that the phase and group velocities differ. In the following, we will always consider the case in which the horizon is a blocking point for the *group* velocity of light, in line with the generally accepted opinion that this kind of horizon is the analogue for photons (or waves in a flowing medium) of a gravitational event horizon.

3. Horizons in dispersive media

We now study how an input wave behaves when interacting with such horizons. This behaviour is analysed by performing numerical simulations based on Maxwell's equations, discretized and solved following the so-called pseudospectral-space-domain technique [28] that is a variation of the more common FDTD technique [29] and allows us to include arbitrary material dispersion in a very simple manner. In more detail, we consider one-dimensional propagation modelled by the Maxwell equations for the transverse x and y components of the electric (E_x) and magnetic fields (H_y), respectively:

$$\partial_z E_x = -\mu_0 \partial_t H_y \tag{1}$$

$$\partial_z H_y = -\partial_t D_x. \tag{2}$$

The electric displacement field is numerically evaluated as $D_x(t) = \mathcal{F}^{-1}\{\varepsilon(\omega)\mathcal{F}[(1 + \varepsilon(z - vt))E_x(t)]\}$, where $\mathcal{F}$ and $\mathcal{F}^{-1}$ indicate the Fourier and inverse Fourier transforms and $\varepsilon(\omega)$ is the dispersive part of the medium refractive index, $n_0 = \sqrt{\varepsilon}$. The moving refractive perturbation is described by a super-Gaussian function $\varepsilon(z - vt) = \varepsilon_0 \exp[-(z - vt)^{2m}/\sigma^{2m}]$, where m is the super-Gaussian order and controls the perturbation steepness and σ gives the perturbation width, typically fixed at 50 μm. The black hole cavity is constructed by using two such perturbations, displaced along the ζ-axis by a distance L that fixes the cavity length (see figure 3). The input seed laser pulse is made to start directly inside the cavity and has the
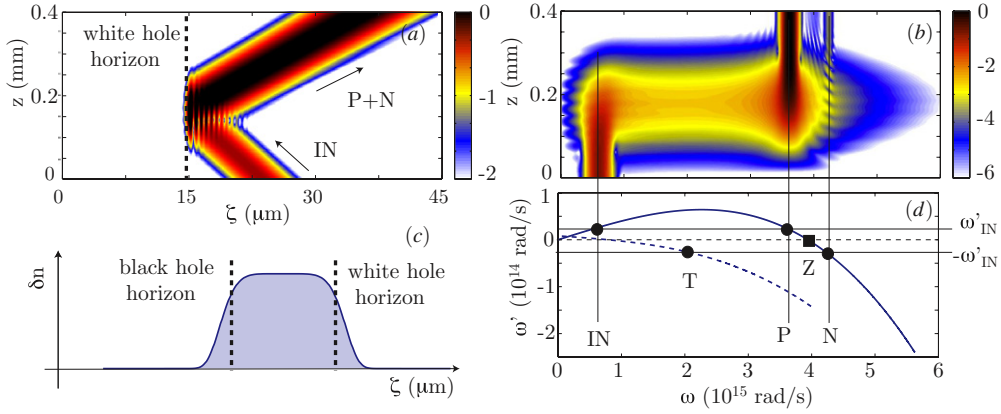
Figure 1. Numerical simulations of the interaction of a laser pulse with a white hole horizon. (*a*) Amplitude profile, in logarithmic scale, of the laser pulse reflecting on the horizon (dashed line). (*b*) Evolution (along the propagation direction, *z*) of the spectrum, in logarithmic scale, during reflection from the horizon. (*c*) Schematic overview of the geometry of a generic refractive index perturbation used in this work and location of the black and white hole horizons. (*d*) Dispersion curve used in this work with indicated positions of the IN (input), P (positive), N (negative), Z (zero-frequency) and T (transmitted) modes. All modes are determined by the condition that frequency is conserved in the comoving frame, i.e. by the intersections of horizontal lines passing through the IN mode frequency, $\pm\omega_{\text{IN}}$.

functional form $E(z-vt) = \exp\left[-(z-vt)^2/\sigma_E^2\right]\cos(kz-\omega t)$, where the initial pulse width σ_E is always taken to be shorter than the cavity length L, e.g. $\sigma_E \sim 3-6\,\mu$m and $L \sim 20-80\,\mu$m. The photon numbers generated at each frequency are evaluated as $S(\omega, z)/\omega$, where $S(\omega, z)$ is the spectral intensity evaluated at each propagation distance, z. Total output photon numbers are obtained by integrating this quantity over frequency. The code was implemented with a dispersion relation shown by the solid line in figure 1(*d*) in (ω', ω) coordinates, where $\omega' = \omega - vk$, with $k = (\omega/c)n(\omega)$, is the frequency in the comoving reference frame. As can be seen, we are using a simplified dispersion curve that does not present any of the typical resonances present in most media such as glass. However, it was chosen to qualitatively reproduce the dispersion of diamond, a material that is currently becoming rather popular for a variety of reasons, including its remarkable transparency range due precisely to the absence of material resonances from sub-THz wavelengths up to the near-UV. Most importantly, such a choice allows us to study the generic physics underlying the black hole laser without additional complications due to specific structures within the dispersion relation.

Figures 1(*a*) and (*b*) illustrate the behaviour at a white hole horizon: the input mode IN is chosen with a low frequency (3 μm wavelength) such that it travels with positive group velocity in the comoving frame (the IN mode identified on the dispersion curve in (*d*) has positive gradient) and therefore catches up with the travelling δn. Upon reaching the horizon, light is blocked and transformed into two new modes, one with a positive frequency, *P*, and one with a negative frequency, *N*. These both have negative group velocity in the comoving frame and are therefore reflected away from the horizon (see (*a*)). These two modes are the Hawking modes generated at the horizon. Most importantly we have explicitly verified that, in agreement with the interpretation in terms of Hawking emission, these two modes are such that the difference of their squared norms (i.e. their photon numbers) is equal to 1, $|P|^2 - |N|^2 = 1$ and the ratio of the squared norms decays exponentially with increasing comoving frequency, $|N|^2/|P|^2 \propto \exp(-C\omega')$, where $C = [(2\pi c)/(\gamma^2 v^2)]1/(\text{d}\delta n/\text{d}\zeta)$ is the decay constant and

dδn/dζ is the perturbation gradient evaluated at the horizon [13, 14]. These two relations imply that the horizon emission in the P mode exhibits a Planckian blackbody spectrum as a function of frequency. Most importantly for the black hole laser, the first relation also implies that the total photon number in reflection from the white hole horizon $|P|^2 + |N|^2 > 1$, i.e. the white hole horizon acts as an amplifying mirror. For small frequencies the photon gain $|P|^2 + |N|^2$ scales as $1/C\omega'$, i.e. the steeper the gradient, the larger the horizon gain will be. This simple recipe is important in order to understand and optimize black hole lasers.

The behaviour of the black hole horizon can be inferred from that of the white hole, as one is the time-inverted version of the other. This implies that a single mode impinging on the black hole horizon will not lead to negative mode generation or, more generally, to positive/negative mode mixing. The P mode will simply convert to the IN mode and reflect away from the black hole horizon. The N mode, on the other hand, will convert to a second redshifted mode that still has negative group velocity and is thus transmitted through the horizon. This transmitted mode is indicated with 'T' in figure 1(*d*). (The dashed dispersion curve is relative to the region inside the black hole.)

Mode mixing and amplification at the black hole horizon will occur if both positive and negative modes, e.g. the same modes generated at the white hole horizon shown in figure 1(*a*), are sent on to the horizon as initial input conditions. In this case we indeed have the time-reversed situation of the white hole horizon. However, as pointed out in [19], this amplification now relies critically on the phases between the P and N modes. For the case of large bandwidth pulses such as those used here, some frequency components will have the correct phase for amplification, whilst others will have the wrong phase. Moreover, it is extremely difficult to purposely control these phases due to the varying and relatively strong dispersion (i.e. accumulated phases in traversing the cavity) across the pulse spectrum. We find that on average the P and N modes meeting at the black hole horizon lead to amplification, although this amplification is typically smaller than that occurring at the white hole horizon.

In the black hole laser configuration discussed below, the white hole horizon will be approached by a single IN mode, whilst the black hole horizon will always be approached with a simultaneous combination of both P and N modes, i.e. the modes generated at the white hole horizon. Therefore, both horizons will act as amplifying mirrors.
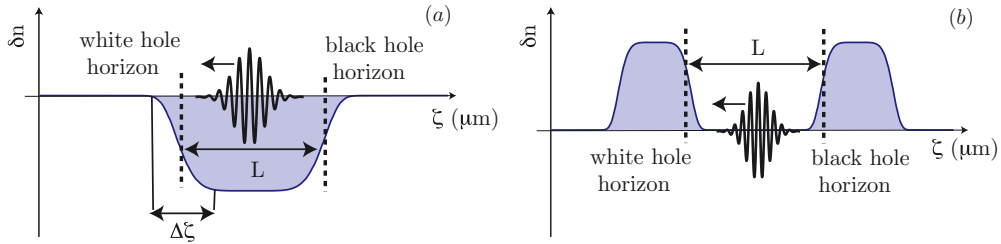
4. The optical black hole laser

On the basis of this reasoning we can construct an intuitive picture of the behaviour of a black hole laser. The black hole laser is formed by placing a black hole horizon and a white hole horizon in close vicinity such that waves are trapped between the two. In order for this to happen care must be taken in choosing the correct arrangement and this depends on the dispersion. In previous studies based on phonon oscillations in BECs, a so-called superluminal dispersion was considered, i.e. the dispersion curve had a positive curvature [18–21]. In our case, we have a dispersion curve with a negative curvature and so-called subluminal dispersion. This implies that in the laboratory reference frame, the group velocity of light is always smaller than the phase velocity and also that it decreases with increasing frequency. Therefore, based on the results in figure 1, if we want to trap light between two horizons, then the white hole horizon must be placed before (at smaller ζ) the black hole horizon.

We illustrate this situation in figure 2 that shows a numerical simulation of the first few cavity round trips of a laser pulse trapped between two horizons. The spectrum evolves periodically at each reflection from the horizon mirrors. We clearly observe the same P and N modes seen in figure 1 at the white hole horizon. At the black hole horizon, the spectrum returns to the original input frequency with the addition of a second very weak, less redshifted
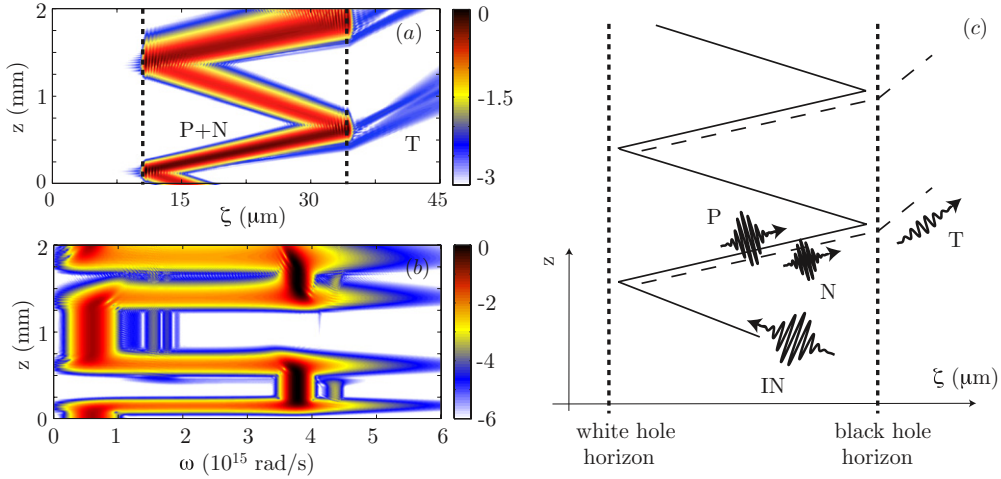
Figure 2. Evolution of a laser pulse during the first few bounces from a white–black hole cavity (logarithmic scale). (*a*) Evolution along the propagation direction, *z*, of the amplitude in the comoving frame as the pulse bounces back and forth. (*b*) Evolution of the pulse spectrum. (*c*) Schematic representation of the cavity behaviour and indication of the various modes that are produced during each round trip.


Figure 3. Possible configurations of the optical black hole laser in the presence of subluminal dispersion. The seed laser pulse is injected directly in the cavity and then propagates first towards the white hole horizon (as indicated by the arrows).

mode around $\omega = 1.5 \times 10^{15}$ rad s^{-1}. This is the 'T' mode mentioned in the previous section (see also figure 1(*d*)) that originates from the partial transmission of the N mode through the black hole horizon and is ejected from the cavity. This mode is also visible in figure 2(*a*), although due to its very low intensity it does not play an important role in the laser dynamics reported in this work. A schematic representation of all the laser modes is shown in figure 2(*c*) that summarizes the behaviour of the light pulse within the cavity and the interaction with the two horizon mirrors.

We note that it is possible to achieve a black hole laser in two ways as shown in figure 3. (a) We may use a negative δn, similar to a potential well which will trap light. This is somewhat difficult to achieve if we assume that the δn is generated by a laser pulse through the Kerr effect due to the fact that most media have positive n_2. Alternatively, (b) we may obtain the same effect by using two positive-valued perturbations generated by two independent laser pulses that are placed a certain distance apart.

As an illustrative case, we show in figure 4 the numerical results for a black hole laser that is obtained using a negative δn ($\delta n_{max} = -0.1$) in which the black and white hole
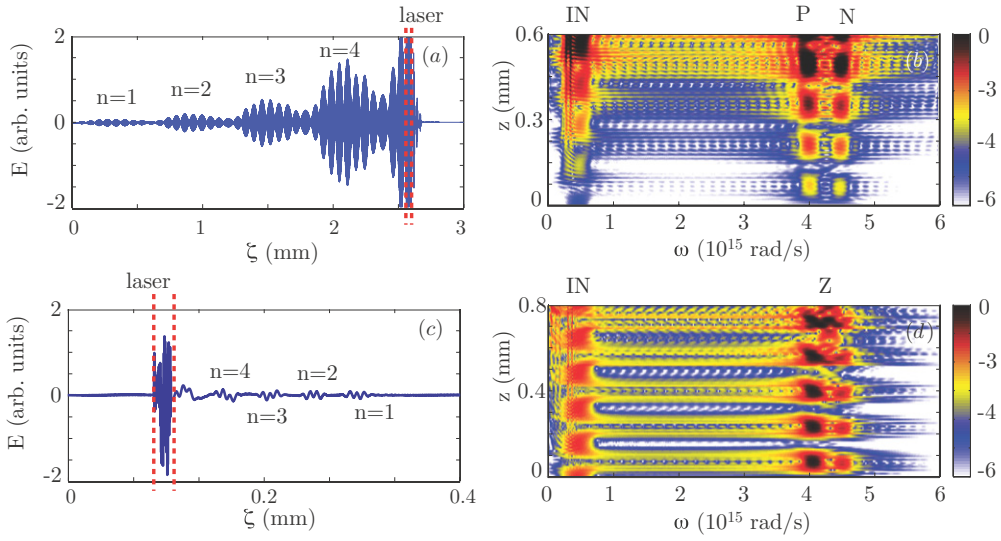
Figure 4. Evolution of the laser spectrum (in log scale) and electric field amplitude at the simulation output are shown for two different cases. (*a*) and (*b*) $\Delta\zeta = 0.3$ μm, and (*c*) and (*d*) $\Delta\zeta = 3$ μm. All other parameters are identical for both simulations: input wavelength 2 μm, cavity length L = 20 μm, $\delta n_{max} = 0.1$.

horizons are separated by 4.5 μm. The input mode is a Gaussian-shaped pulse, with 3 μm carrier wavelength and pulse length of 2 cycles. Figure 4(*a*) shows the electric field in the vicinity of the black hole laser after a propagation distance of 650 μm. The vertical dashed lines indicated the position of the cavity that is travelling from left to right. The input mode, originally localized only within the cavity has led to lasing in the form of bursts of pulses tunnelling and exiting through the white hole horizon (not to be confused with the T-mode that would exit the black hole horizon yet is too weak to be seen in this simulation). These bursts are composed of a sum of both P and N modes (hence the beat signal that modulates the individual bursts) and occur once every cavity round trip, indicated with $n = 1, 2, 3, 4$ in the figure. These bursts are strongly increasing in amplitude at each round trip, a clear indication of the gain provided by the black hole laser. We note that here the modes leaking out of the cavity are doing so as a result of a tunnelling effect: the refractive index increase from the background to the maximum value (denoted by $\Delta\zeta$ in figure 3(*a*)) at the white hole horizon occurs over a distance that is shorter than the optical wavelength. The modes therefore tunnel out of the hole—this tunnelling may be controlled by reducing the gradient of the refractive index profile and indeed, for refractive index changes that occur over scales larger than the mode wavelength, the outgoing leakage is suppressed and the modes are completely trapped within the cavity (see below). Figure 4(*b*) shows the spectral evolution corresponding to figure 4(*a*): the periodic back and forth conversion between the IN and P/N modes at each cavity round trip can be clearly seen with a gain of more than five decades after only $n = 4$ round trips. These findings are qualitatively similar to those reported for black hole lasers in BECs [19]. However, such a setting will be experimentally challenging both in virtue of the large δn (although similar results were obtained with smaller δn, at the cost of correspondingly longer propagation distances) and of the extremely short distances at play, i.e. the short separation between the horizons and sharp $\Delta\zeta$ increase at the horizon from the background index to the maximum δn.

In figures 4(*c*) and (*d*) we show the same simulation with a transition $\Delta\zeta$ that has been reduced to experimentally reasonable values, i.e. $\Delta\zeta \sim 3~\mu$m. As can be seen, the high-frequency modes no longer leak out of the white hole horizon. This allows for a higher gain within the cavity itself, although this is largely counterbalanced by the detrimental effect of reducing the δn gradient as this reduces the amplification at each reflection. Nevertheless, in this situation a stronger build-up of negative frequencies occurs inside the cavity, which partly leak out from the black hole horizon at each round trip in the form of a more intense and now visible 'T' mode, as discussed in figure 1(*d*). The T mode is emitted in bursts corresponding to the cavity round-trips (indicated with $n = 1, 2, 3, 4$ in the figure).

Finally, we note that in the very last stages of this simulation we can clearly see that the spectrum is starting to exhibit two distinct and new features: a strongly redshifted component close to $\omega = 0$ and a component, indicated with Z, that lies in between the P and N modes. In the following, we focus attention on these new modes and highlight a new mechanism by which the pulse spectrum is broadened at each bounce until far-infrared wavelengths are generated. These then seed and sustain amplification at the zero-frequency points of the dispersion curve (indicated with filled squares in figure 1(*d*)), which have a gain favoured by the aforementioned $1/\omega'$ dependence. This results in remarkably stronger gain and significant lasing even under conditions that could be realized in experiments.

4.1. Zero-frequency mode amplification

Figures 5(*a*) and (*c*) show results from a simulation in which the first several cavity round trips are shown. The horizon separation is 80 μm, with 2 μm input wavelength, $\Delta\zeta = 3~\mu$m, $\delta n = 0.01$—the curves are normalized and displaced horizontally for viewing purposes. The optical modes bounce back and forth but without any apparent overall increase in energy for nearly the first mm of propagation. At $z = 0.8$ mm, a series of relatively weak bursts are clearly visible corresponding to T mode emission from the black hole horizon at each round trip. Figure 6(*a*) shows the total photon number inside the cavity. During the first ~ 1 mm or propagation, the energy inside the cavity oscillates. These initial oscillations do not appear to be a numerical artefact and seem to correspond to real light pulse dynamics within the cavity. They most likely arise from a beating between the different modes that are concomitantly excited within the cavity and that therefore interfere with each other giving rise to amplitude oscillations, in a similar fashion to the build-up dynamics that may be observed in traditional laser cavities. After this short transitory period, a different regime appears in which the energy oscillations are washed out by a smooth and strong exponential increase of the total energy in the cavity. The origin of this change in behaviour can be understood from figure 5(*a*). During the first mm of evolution, light bounces back and forth but is gradually spread out to very low frequencies. This low-frequency light has two effects: (i) due to its long wavelength it will start to completely fill the cavity and (ii) it will seed mode conversion to high-frequency modes that lie close to or at the intersection of the dispersion curve with the horizontal axis, i.e. it will excite modes that have $\omega' \to 0$, indicated with filled squares in figure 5(*b*). (We name the high-frequency intersection as the 'Z' mode.) In order to understand why these zero-frequency modes appear we recall that, as a consequence of the Planckian distribution of Hawking emission, amplification at the horizon diverges as $1/\omega'$ for small ω'. Therefore, the laser gain experienced by these very low frequency modes is remarkably stronger with respect to all other modes and they will therefore quickly take over: high-gain lasing at the 'zero frequencies' will, and is expected to dominate the black hole laser scenario.

In figure 6(*b*), we show the cavity photon number for identical operating conditions and with varying maximum δn amplitude, as indicated in the figure. The gain (slope of the curve)
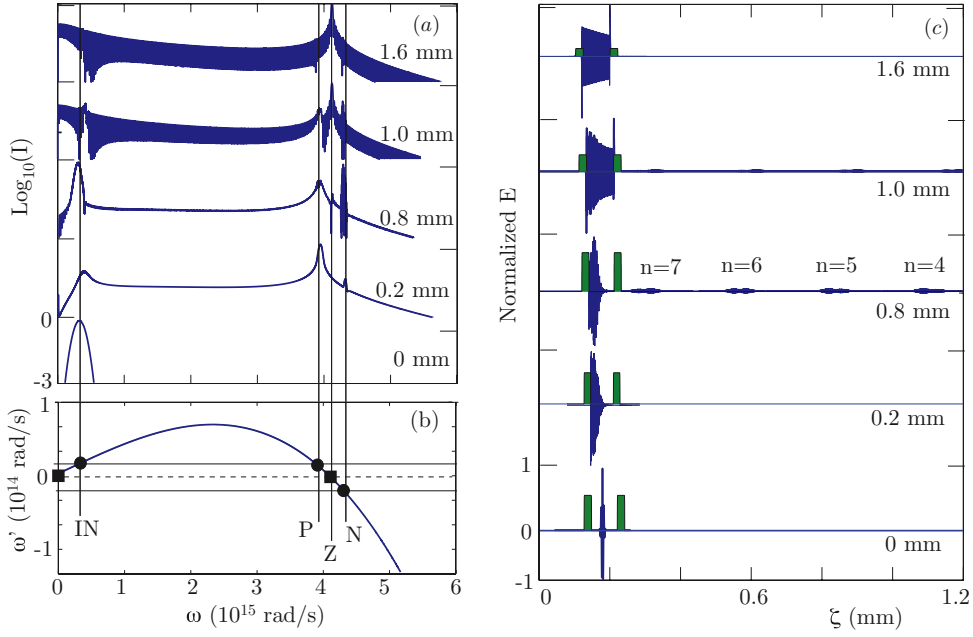
Figure 5. Evolution of the normalized laser spectrum (in logarithmic scale, three decades) and normalized electric field amplitude (linear scale, from -1 to $+1$)—profiles are shown for increasing propagation distances as indicated in the graphs. Each 0.1 mm of propagation corresponds very closely (in this simulation) to one cavity round trip. Parameters used in the numerical simulations are: input wavelength of 2 μm, $\Delta\zeta = 3\ \mu$m, cavity length $L = 80\ \mu$m, $\delta n_{\max} = 0.01$. The shaded regions in (c) indicate the position and (rescaled) shape of the two δn perturbations forming the cavity.
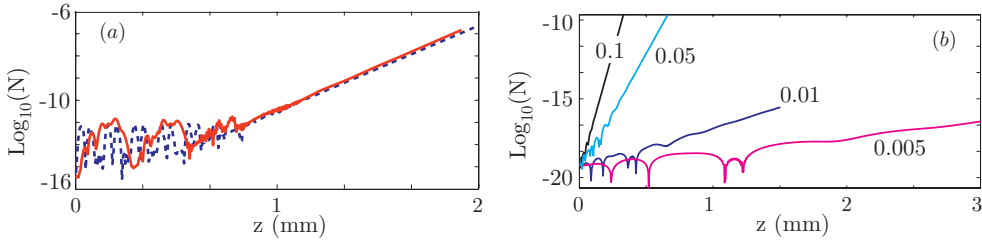
Figure 6. (a) Evolution of the photon number N (in logarithmic scale) inside the black hole laser cavity for a δn amplitude of 0.01 and two different configurations shown in figure 3 (solid line—negative δn, dashed line—positive δn). (b) Photon number inside the laser cavity for various maximum δn amplitudes, indicated in the graph.

is seen to decrease with decreasing δn amplitude as a result of the fact that we have fixed the distance over which the perturbation switches on, $\Delta\zeta = 3\ \mu$m. Therefore, the horizon gradient (i.e. surface gravity) and hence also the horizon amplification decrease with decreasing $\delta n_{\max}$. Nevertheless, a significant laser gain is observed even at low perturbation amplitudes that hold promise for future experiments.

The question now arises as to how close to zero in the laboratory frame does the $\omega \to 0$ zero-frequency mode have to be in order for this process to occur? The question is relevant
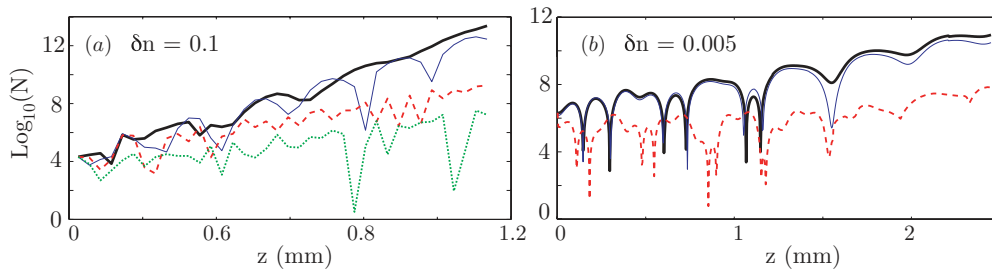
Figure 7. Evolution of the photon number inside the cavity for (*a*) $\delta n = -0.1$ and (*b*) $\delta n = -0.005$. The simulations were performed by including a spectral filter that cuts all frequencies below a certain value. The shortest propagating wavelengths are (*a*) thick solid line—no filter, thin line—20 μm, dashed line—8 μm, dotted line—4 μm. In (*b*) thick solid line—no filter, thin line—60 μm, dashed line—10 μm.

as real experiments cannot be expected to rely on modes for example in the radio frequency domain. We therefore repeated the simulations by including a low-frequency filter so as to completely suppress all radiation below a certain threshold value. Figure 7(*a*) shows the results for a δn amplitude of 0.1 and filters as indicated in the caption. As may be seen, a filter placed at a wavelength of 20 μm hardly modified the overall gain, and a reduction of ∼50% is obtained only when the filter is placed at a wavelength of 8 μm. In figure 7(*b*), we repeat the simulations for an experimentally realistic δn amplitude of 0.005. A filter placed at 60 μm does not modify the laser gain and a 50% cut is observed with a filter placed at 10 μm. This is extremely promising. Indeed, many media are transparent in to the terahertz region (30–100 μm). For example diamond is transparent up to roughly 100 μm. This would therefore seem to indicate that this kind of novel amplification process could be observed in real settings.

5. Conclusions

We have numerically analysed the possibility of observing black hole lasing using laser-pulse-induced (or optical) horizons. The general behaviour of the black–white hole horizon cavity is very similar to the behaviour of similar cavities studied theoretically and numerically in BECs. Our numerical simulations have been carried out over longer propagation distances (i.e. a larger number of cavity round-trips) with respect to previous studies and highlight the onset of a regime in which the cavity leads to a broadening of the mode spectra until the two comoving zero-frequency modes are excited. (In the laboratory frame, one mode lies at zero-frequency, the other lies in the visible or ultraviolet region, depending on the specific dispersion relation of the medium.) Due to the $1/\omega'$ dependence of the horizon amplification, the zero-frequency modes oscillate in the cavity with a much higher gain. These findings are summarized in the accompanying video animation (available from stacks.iop.org/CQG/29/000000/mmedia) that shows the evolution of the typical situation studied here: the initial optical pulse seeded in to the cavity is actually much shorter than the cavity itself (differently from typical cases studied so far in which the cavity length was of the same order of the input wavelength) and bounces back and forth until the zero-frequency modes take over and completely fills the cavity.

Our numerical simulations treat the case of a coherently seeded laser. Naturally, one would expect that if the laser were to be seeded by vacuum fluctuations, then most certainly laser oscillation would occur at the zero-frequency modes as these have the highest gain and lowest lasing threshold.

A remarkable and unique feature of black hole lasers is the coupling between the very low frequency and very high frequency components of the electromagnetic spectrum. However, more complicated dispersion relations that include also resonances at certain wavelengths are expected to complicate this picture, although a full model that includes losses due to material absorption would be required in order to correctly model such a situation.

These simulations underline the fact that an experimental demonstration of black hole lasing, although not simple may not be as far-fetched as one may think. Refractive index perturbations of the order of 0.005 (or smaller) will give rise to a significant gain over distances of the order of 1 cm. The dispersion relation used in this work is very close to that of diamond, a material that is now widely used and can be shaped into optical waveguides. Diamond exhibits not only a very simple dispersion curve but also (as a consequence of this) a remarkably wide transparency range that could easily sustain the zero-frequency amplification regime reported here. The laser cavity, i.e. the black and white hole horizons could be generated by focusing for example two independent and ultrashort laser pulses, e.g. at 800 nm wavelength: each pulse would create a δn through the nonlinear Kerr effect, and the relative delay between the two pulses would allow us to control the laser cavity length. The main challenge would be to find a condition (laser wavelengths, durations, energies) such that the rising and falling edges of the laser pulses that form the horizons are maintained shorter than $\sim 3~\mu$m for significantly long propagation distances, e.g. $> 1 - 2$ mm. Future studies will, we hope, unravel other settings or combinations of materials and wavelengths that may indeed lead to the first experimental black hole laser. In the meantime, this remains a fascinating scenario in which to combine technologies and ideas developed in the area of photonics to the study of flowing media and horizon physics.

Acknowledgments

References

[1] Unruh W G 1981 Experimental black-hole evaporation? *Phys. Rev. Lett.* **46** 1351–53
[2] Novello M, Visser M and Volovik G E 2002 *Artificial Black Holes* (Singapore: World Scientific)
[3] Barceló C, Liberati S and Visser M 2011 Analogue gravity *Living Rev. Rel.* **14** 1–179
[4] Hawking S W 1974 Black hole explosions? *Nature* **248** 30–1
[5] Hawking S W 1975 Particle production by black holes *Commun. Math. Phys.* **43** 199–220
[6] Philbin T G, Kuklewicz C, Robertson S, Hill S, König F and Leonhardt U 2008 Fiber-optical analog of the event horizon *Science* **319** 1367
[7] Hawking S W 1976 Black holes and thermodynamics *Phys. Rev.* D **13** 191–7
[8] Rousseaux G, Mathis C, Maïssa P, Philbin T G and Leonhardt U 2008 Observation of negative-frequency waves in a water tank: a classical analogue to the Hawking effect *New J. Phys.* **10** 053015
[9] Weinfurtner S, Tedford E W, Penrice M C J, Unruh W G and Lawrence G A 2011 Measurement of stimulated Hawking emission in an analogue system *Phys. Rev. Lett.* **106** 021302
[10] Faccio D, Cacciatori S L, Gorini V, Sala V G, Averchi A, Lotti A, Kolesik M and Moloney J V 2010 Analogue gravity and ultrashort laser pulse filamentation *Europhys. Lett.* **89** 34004
[11] Demircan A, Amiranashvili Sh and Steinmeyer G 2011 Controlling light by light with an optical event horizon *Phys. Rev. Lett.* **106** 163901
[12] Choudhary A and König F 2012 Efficient frequency shifting of dispersive waves at solitons *Opt. Express* **20** 5538
[13] Belgiorno F, Cacciatori S L, Ortenzi G, Rizzi L, Gorini V and Faccio D 2011 Dielectric black holes induced by a refractive index perturbation and the Hawking effect *Phys. Rev.* D **83** 024015

11

[14] Rubino E, Belgiorno F, Cacciatori S L, Clerici M, Gorini V, Ortenzi G, Rizzi L, Sala V G, Kolesik M
     and Faccio D 2011 Experimental evidence of analogue hawking radiation from ultrashort laser pulse filaments
     New J. Phys. **13** 085005
[15] Schützhold R and Unruh W G 2011 Comment on hawking radiation from ultrashort laser pulse filaments *Phys.
     Rev. Lett.* **107** 149401
[16] Belgiorno F, Cacciatori S L, Clerici M, Gorini V, Ortenzi G, Rizzi L, Rubino E, Sala V G and Belgiorno D Faccio
     et al 2011 *Phys. Rev. Lett.* **107** 149402
[17] Liberati S, Prain A and Visser M 2012 Quantum vacuum radiation in optical glass *Phys. Rev. D* **85** 084014
[18] Corley S and Jacobson T 1999 Black hole lasers *Phys. Rev. D* **59** 124011
[19] Leonhardt U and Philbin T G 2007 Black-hole lasers revisited *Quantum Analogues: From Phase Transitions
     to Black Holes and Cosmology* ed W G Unruh and R Schutzhold (Berlin: Springer)
[20] Coutant A and Parentani R 2010 Black hole lasers, a mode analysis *Phys. Rev. D* **81** 084042
[21] Finazzi S and Parentani R 2010 Black hole lasers in Bose–Einstein condensates *New J. Phys.* **12** 095015
[22] Faccio D 2012 Laser pulse analogues for gravity and analogue Hawking radiation *Contemp. Phys.* **53** 97–112
[23] Boyd R W 2008 3rd edn (Academic Press)
[24] Gordon W 1923 Zur lichtfortpflanzung nach der relativitätstheorie *Ann. Phys., Lpz.* **377** 421
[25] Cacciatori S L, Belgiorno F, Gorini V, Ortenzi G, Rizzi L, Sala V G and Faccio D 2010 Spacetime geometries
     and light trapping in travelling refractive index perturbations *New J. Phys.* **12** 095021
[26] Painlevé P 1921 La mécanique classique et la théorie de la relativité *C. R. Acad. Sci.* **173** 677
[27] Gullstrand A 1922 Allgemeine lösung des statischen einköperproblems in der Einsteinschen gravitationstheorie
     Arkiv. Mat. Astron. Fys. **16** 1–15
[28] Tyrrell J C A, Kinsler P and New G H C 2005 Pseudospectral spatial-domain: a new method for nonlinear pulse
     propagation in the few-cycle regime with arbitrary dispersion *J. Mod. Opt.* **52** 973–86
[29] Taflove A and Hagness S C 2005 *Computational Electrodynamics: The Finite-Difference Time-Domain Method*
     3rd edn (Norwood, MA: Artech House)